

SUBSEA CABLE TRENCHER PERFORMANCE ON SAND DUNES

NUMERICAL MODELLING OF THE WATERJET TRENCHING
PROCESS AND VEHICLE TRACTION ON SAND DUNES

S.H. Warringa



SUBSEA CABLE TRENCHER PERFORMANCE ON SAND DUNES

NUMERICAL MODELLING OF THE WATERJET TRENCHING
PROCESS AND VEHICLE TRACTION ON SAND DUNES

by

S.H. Warringa

to obtain the degree of Master of Science
at the Delft University of Technology,
to be defended publicly on Tuesday August 28, 2018 at 9:30 AM.

Student number: 4421345
Project duration: December 4, 2017 – August 28, 2018
Thesis committee: Dr.ir. S. A. Miedema, TU Delft, Chairman
Prof.dr.ir. C. van Rhee, TU Delft, Committee member
Dr.ir. M. van Damme, TU Delft, External committee member
Ir. C. Visser, Tideway Offshore Solutions, Supervisor
Ir. C. Lupea, Tideway Offshore Solutions, Daily Supervisor

This thesis is confidential and cannot be made public until August 28, 2023.

An electronic version of this thesis is available at <http://repository.tudelft.nl/>.

Abstract

DELFT UNIVERSITY OF TECHNOLOGY
TIDEWAY OFFSHORE SOLUTIONS

Master of Science Offshore and Dredging Engineering
Subsea cable trencher performance on sand dunes
by S.H. Warringa

Numerous offshore wind farms have been constructed recently in the southern part of the North Sea. Their infield and export cables are buried for protection against dropped or dragged objects. In sandy soils, it is common to use tracked remotely operated vehicles, equipped with two water jetting swords. These swords fluidise the seabed and generate a backward flow of water-sediment mixture, allowing the cable to sink into the seabed. The southern part of the North Sea has a highly variable seabed topography characterised by sandwaves and megaripples. These seabed features have a significant influence on the trenching process. Existing models do not allow for an accurate estimation of the influence of seabed slopes on the trenching process and are often not based on fundamental physical processes. Two separate numerical models are developed; a jet trenching model describing the cable burial process and a traction model describing the seabed trafficability.

The jet trenching model is divided into three parts; an erosion model describing the erosion of soil by the waterjets, a sedimentation model describing the re-sedimentation process and resulting trench shape and a cable model describing the cable deflection. The erosion and sedimentation model combined describe the flow of water and sediment in the trench. The erosion model is based on a specific energy approach to determine the maximum allowable trencher velocity, limited by the eroding capacity of the jets. The sedimentation model describes the flow of water-sediment mixture through a rectangular channel, based on the shallow water equations. The channel width is able to evolve due to breaching and the bed elevation is controlled via erosion and sedimentation. The shallow water equations are solved on a staggered grid, following a one-dimensional finite volume scheme. A moving boundary is imposed on one side of the grid to simulate trencher movement. Seabed topography can be imported to model trencher performance on sand dunes.

Tractive performance of the vehicle is modelled by considering its driving state. A constant velocity is assumed, hereby balancing thrust and resistance forces. Resistances due to static sinkage, slip sinkage, seabed slopes, current and internal running gear friction are included. The driving thrust force is found by integration of shear stress over track-seabed contact area, including effects of slippage and constant seabed slopes.

A sensitivity study has been performed on the jet trenching model, where a strong influence on achieved depth of lowering was found to be caused by grain sizes and depth of the jetting sword below seabed. Influence of trencher velocity on depth of lowering was found to be associated with grain sizes. A higher trencher velocity has a positive effect on the achieved depth of lowering in coarse sand, whereas in fine sand the trencher velocity has a negligible influence on the depth of lowering. Validation of the model with field data shows reasonable agreement regarding average depth of lowering. When including sand dunes, results of the model show a similar depth of lowering trend as observed in field data. However, the amplitude of depth of lowering variation is underestimated by the model.

The sensitivity study performed on the traction model showed that resulting slip ratio and power demand have a strong dependency on track-seabed contact area and corresponding normal pressure distribution. Work remains to include the effect of variable seabed slopes, since the current model is based on constant seabed slopes.

Preface

This master thesis is the ultimate result of the time I spent studying at the Delft University of Technology. The completion of this thesis also marks the completion of the master programme Offshore and Dredging Engineering. During the past nine months I was able to investigate and model the performance of a subsea cable trencher on sand dunes, a research topic initiated by Tideway Offshore Solutions.

Firstly, I would like to express my gratitude toward Tideway in general and specifically to Connie Visser for the opportunity to do this thesis at Tideway's engineering department. Also I would like to thank Cristina Lupea for her role as daily supervisor, providing me with plenty of input and feedback. Furthermore, I would like to thank my Tideway colleagues for their help, suggestions and general support during the past nine months.

Secondly, I would like to express my appreciations towards my university supervisors Sape Miedema and Cees van Rhee for their time. Their input, tips and feedback form an essential basis for the achieved result.

Last but not least I would like to express my gratitude to my friends and family for their support and encouragement. Not only during the last nine months but throughout my entire study period, their unconditional support has helped me a lot.

*S.H. Warringa
Breda, August 2018*

Contents

Abstract	iii
Preface	v
Contents	viii
List of Figures	ix
List of Tables	xi
Nomenclature	xiii
1 Introduction	1
1.1 Background	1
1.2 Problem statement	2
1.3 Thesis boundaries	2
1.4 Thesis outline	3
2 Theoretical background	5
2.1 Introduction to the cable trenching process	5
2.1.1 Cable burial definition	5
2.1.2 Cable trenching equipment	5
2.1.3 Cable trenching operations	6
2.1.4 Findings in available data	7
2.1.5 Findings of laboratory model tests	7
2.2 Seabed features	8
2.3 Physical processes during jet trenching	9
2.3.1 Dimensionless numbers	9
2.3.2 Erosion	9
2.3.3 Sedimentation	11
2.3.4 Breaching	11
2.3.5 Entrainment	12
2.3.6 Bed friction	12
2.4 Free turbulent jets	13
2.5 Jetting in sand	14
2.5.1 Stationary jetting in sand	14
2.5.2 Jetting in sand by a translating jet	14
2.5.3 Jet production - Specific energy approach	15
2.5.4 Jet production - C.S.B.	16
2.5.5 Jet production - Vlasblom	17
2.5.6 Comparison jet production models	17
2.6 Soil mechanics	18
2.6.1 Mohr-coulomb failure criteria	18
2.6.2 Shear stress-displacement behaviour	18
2.6.3 Soil stress distribution under uniform strip load	20
2.7 Specific energy	20
2.8 Track belt theory	21
2.8.1 Rigid versus flexible track belts	21
2.8.2 Grousers	21
2.8.3 Slip	21
2.8.4 Slip sinkage	22

3	Jet trenching model	23
4	Traction model	25
5	Results and discussion	27
6	Conclusions and recommendations	29
	Bibliography	31
	Appendices	33
A	Trencher specifications (CBT-1100)	35
B	Trenching process identification	37
C	Results of cable deflection model verification with OrcaFlex	39
D	Second pass trenching	41

List of Figures

1.1	Snapshots from 3D animations of a cable plough (a), trencher with chain cutter (b) and trencher with jetting swords (c). (Image source: Soil Machine Dynamics Ltd.)	1
1.2	Illustration of working principle of the jet trenching system, showing depth of lowering (DOL) definition.	2
2.1	Various definitions used to indicate the burial depth of a subsea cable [DNV-GL, 2016].	5
2.2	Experimental results by [Vanden Berghe et al., 2011], re-scaled from experimental scale to prototype scale.	7
2.3	Side view of waterjet trenching experiments, carried out at the National University of Taiwan in collaboration with CTC Marine Projects and Fugro Engineers SA [Vanden Berghe et al., 2008].	8
2.4	Key physical processes during jet trenching [Vanden Berghe et al., 2011].	9
2.5	(a) Graphical representation of increase in pore volume (dilatancy) and decrease in pore volume (contraction). (b) Demonstration of the breaching process. [van Rhee, 2017]	12
2.6	Entrainment coefficient as a function of Richardson number for various empirical relations.	13
2.7	Sketch showing the flow field of a circular turbulent jet, including the corresponding definitions. Image from [Nobel, 2013].	13
2.8	Velocity development along jet centerline.	14
2.9	Two different options of scour hole profiles for stationary jets, depending on pressure parameter p_p [Kobus et al., 1979].	15
2.10	Qualitative comparison of trench profiles create by a plane turbulent jet, for varying trailing speeds. Top left; stationary jet, top right; very slowly moving jet, bottom left; slowly moving jet, bottom right; rapidly moving jet. Image by Perng and Capart [2008].	15
2.11	Trench shape ratio α_{CSB} as a function of the transit velocity v_t for two different soil type and hydraulic power combinations. Data points are from research by CSB de Jong [1988].	17
2.12	Maximum trench cross section for the Miedema, CSB and Vlasblom jet production models. Required trench cross section based on a 2m by 0.75m trench.	18
2.13	Mohr-Coulomb failure envelope for a soil with both cohesion and friction.	18
2.14	Shear stress-displacement curve for a loose sand (type 1) [Wong and Preston-Thomas, 1983].	19
2.15	Shear stress-displacement curve (type 2) [Wong and Preston-Thomas, 1983].	19
2.16	Shear stress-displacement curve (type 3) [Wong and Preston-Thomas, 1983].	20
2.17	Stress distribution under uniform strip load.	20
2.18	Flexible type track belt (left) and rigid type track belt (right), image from [Daanen, 2017].	21
2.19	Visualisation of shear displacement initiated by a difference in track and trencher velocity.	21
2.20	Comparison of the slip sinkage relations proposed by Bekker [1956], Reece [1965] and Lysako [2009] for a static sinkage depth of $Z_0 = 0.1\text{m}$ and grouser height of $h_{gr} = 0.1\text{m}$	22

List of Tables

2.1 Nomenclature for seabed formations, suggested by Gass [1984].	8
---	---

Nomenclature

Abbreviations

CFL	Courant-Friedrichs-Lewy
DOL	Depth Of Lowering
FV	Finite Volume
OD	Outer Diameter

Roman symbols

\dot{M}_s	Mass flux	kg/s
A	Area	m ²
B	Track width	m
b	Trench width (breadth)	m
c	Volumetric concentration	-
c_1	Empirical coefficient	-
C_d	Drag coefficient	-
D	Diameter	m
d	Depth	m
E	Erosion flux	kg/m ² s
e	Virtual center of gravity eccentricity	m
E_{sp}	Specific energy	W/m ³ /s
EI	Bending stiffness	Nm ²
F	Force	N
f	Friction coefficient	-
Fr	Froude number	-
G	Trencher weight	N
g	Gravitational acceleration	m ² /s
h	Height	m
i	Slip ratio	-
j	Shear deformation	m
K	Shear deformation modulus	m
k	Seabed permeability	m/s
$k_{0,pp}$	Pressure parameter	-

k_ϕ	Empirical pressure-sinkage constant	-
L	Length	m
m	Mass	kg
n	Seabed porosity	-
P	Power	W
p	Pressure	N/m ²
Q	Flow rate	m ³ /s
q	Weight	N/m
R	Resistance force	N
r	Radius	m
Re	Reynolds number	-
Ri	Richardson number	-
Rp	Particle reynolds number	-
S	Sedimentation flux	kg/m ² s
s	Jet distance, measured along centerline of the jet	m
T	Thrust force	N
t	Time	s
T_{cable}	Residual cable lay tension	N
u	Flow velocity	m/s
v_t	Longitudinal trencher velocity	m/s
v_{lat}	Lateral trencher velocity	m/s
v_{wall}	Active wall velocity due to breaching	m/s
W	Trencher width	m
w	Particle settling velocity	m/s
w_s	Particle settling velocity	m/s
x	Horizontal coordinate	m
y	Horizontal coordinate	m
z	Vertical coordinate	m
Z_0	Static sinkage	m
Z_i	Slip sinkage	m
Greek symbols		
α	Auxiliary factor	-
Δ	Relative density	-
ϵ	Dilatancy	-

ϕ	Trencher or seabed roll angle	deg
ϕ_{fric}	Internal friction angle	deg
Φ_p	Dimensionless pick-up flux	deg
ρ	Density	kg/m ³
σ	Stress	N/m ²
τ	Shear stress	N/m ²
θ	Trencher or seabed pitch angle	deg
ν	Kinematic viscosity	m ² /s

Subscripts

0	Initial
15	15th percentile
50	Median
E	Entrainment
FP	Friction plane
gr	Grouser
j	Jet
L	Left
n	Nozzle
OD	Overdepth
R	Right
s	After re-settling
sed	Sedimentation
sw	Sand wave
t	Trencher
tr	Trench

Introduction

1.1. Background

During the last decade there has been a vast growth in the number of wind turbines being placed offshore. The energy generated by these turbines is transported via cables located on the seafloor. Infield cables transport the energy from individual turbines to an offshore substation (OSS), after which it goes via an export cable to shore. Since the 1970's it became common to bury offshore cable to protect them against dropped or dragged objects, for example caused by fishing activities. Another possibility is to cover the cable by rocks, concrete mattresses or cast iron shells, however this is less common. The cable burial process, referred to as *trenching* in the offshore industry, can be carried out with a variety of equipment. Mostly depending on soil characteristics, the main options are ploughing, mechanical cutting or jetting in the soil to create a trench for the cable. See figure 1.1 for an overview of the most commonly used equipment.

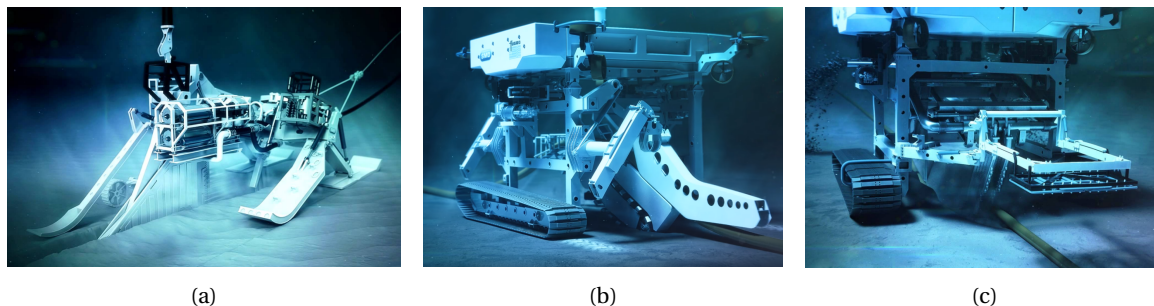


Figure 1.1: Snapshots from 3D animations of a cable plough (a), trencher with chain cutter (b) and trencher with jetting swords (c).
(Image source: Soil Machine Dynamics Ltd.)

Tideway, subsidiary of the Belgian DEME group and sponsor of this thesis, is a company providing a wide range of offshore solutions. Main activities consist of pipeline landfall construction, subsea rock placement, cable installation and offshore dredging. To extend their services, Tideway acquired its own remotely operated trenching vehicle in 2015. The trencher has the capability to bury cables either by jetting, for sandy seabeds, or by using a chain cutter for cohesive seabeds. For the current thesis only the jetting mode is considered. In this operation mode two beams with water jetting nozzles, referred to as *jetting swords*, are lowered into the seabed. The water jets fluidise the seabed underneath the cable, thus allowing the cable to sink into the seabed. After settling of the sand particles the seabed becomes solid again, fixing the cable in its buried position. See figure 1.2 for an illustration of this process.

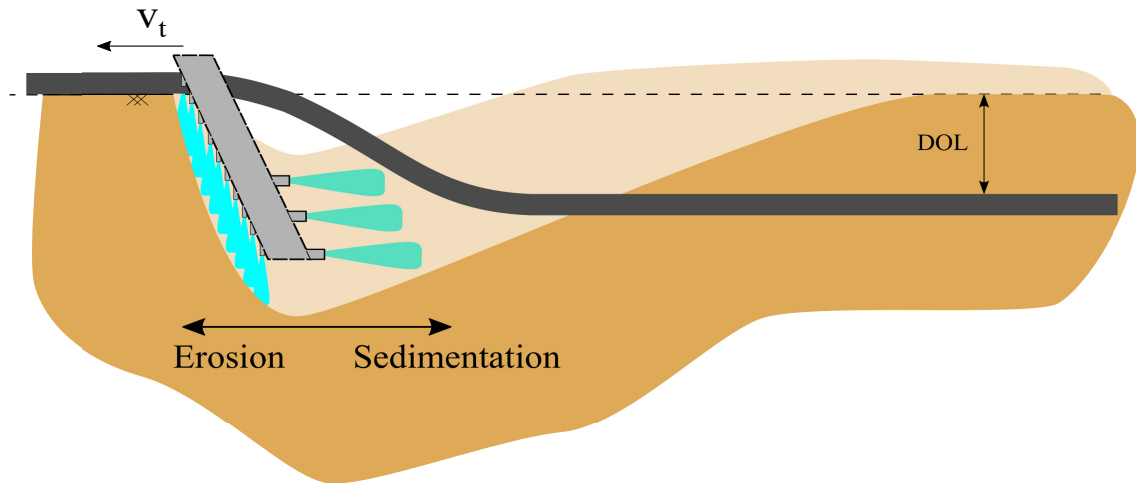


Figure 1.2: Illustration of working principle of the jet trenching system, showing depth of lowering (DOL) definition.

1.2. Problem statement

Not available

1.3. Thesis boundaries

The burial of cables in the seafloor can be a broad topic and is a frequent topic of research. It is therefore required to set clear boundaries to narrow the current research. Therefore throughout the thesis only the jetting sword tool of the trencher is considered. Also it is assumed that the seafloor consists of sand only, consequently the presence of cohesive materials and boulders is not considered. The model should be developed in programming language *Python* since this is the standard within Tideway.

1.4. Thesis outline

Chapter 2 starts with an introduction of the cable trenching process, corresponding definitions and equipment. Following to this introduction all fundamental physical processes are described related to both jet trenching and traction of the tracks.

Chapter 3 contains the description of the jet trenching model, divided in three main sub-models; a model of the erosion section, a model of the suspended sediment flow in the trench, and a model describing the deflection of the cable in the trench.

Chapter 4 is describing the traction model, starting with the mathematical description of the normal pressure distribution. In the next section the resistance forces are elaborated, followed by the maximum available traction. To conclude the chapter, the outputs of the model are described in the last section.

Chapter 5 discusses the results and performance of the model. In the first section a sensitivity analysis is presented, followed by model validation with field data. Results are discussed in the final section.

Chapter 6 summarises the conclusions and recommendations resulting from the thesis.

2

Theoretical background

2.1. Introduction to the cable trenching process

2.1.1. Cable burial definition

The depth of burial of a subsea cable can be defined in various ways, as given in figure 2.1 from the recommended practice by DNV-GL [2016]. Depth of trench is defined as the vertical distance between bottom of trench and undisturbed (mean) seabed level, depth (height) of cover is the vertical distance between top of cable and average level of the backfill above top of the cable. The most commonly used measure is the depth of lowering, which is the vertical distance between top of cable and undisturbed (mean) seabed level. The depth of lowering is considered throughout this thesis and sometimes also abbreviated by *DOL*.

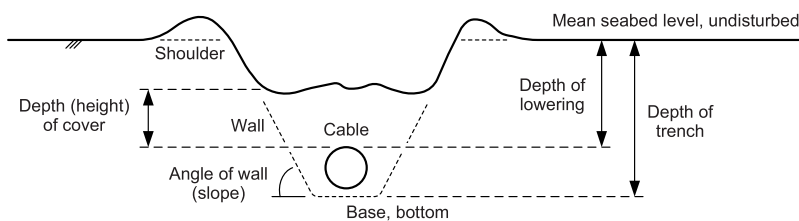


Figure 2.1: Various definitions used to indicate the burial depth of a subsea cable [DNV-GL, 2016].

2.1.2. Cable trenching equipment

Not available

2.1.3. Cable trenching operations

Not available

2.1.4. Findings in available data

Not available

2.1.5. Findings of laboratory model tests

Various series of experiments have been conducted at the National University of Taiwan ([Vanden Berghe et al., 2008], [Perng and Capart, 2008], [Vanden Berghe et al., 2011]). Experiments were conducted in sand with moving point jets, moving plane jets and jetting swords. For the current thesis specifically the experiments with jetting swords are interesting, although unfortunately not all experimental results were published in detail. The key findings of their series of experiments were the following [Vanden Berghe et al., 2011].

- Trench lengths for a certain jetting tool depend mostly on the grain size, but also seabed density has some influence. Fine sands create longer trenches due to lower settling velocities of the grains compared to coarse sands. Denser beds (low porosity) reduce the pace of sidewall breaching and slumping, and thus create longer trenches.
- A downward orientation of the forward jets results in an increase in maximum trench depth, but this increase is localised and does not necessarily translate into an increase in trench length.
- The orientation of the forward jets seems to have little to no influence on the trench profile, for loose beds.
- There is approximately a linear relation between total jet flow and open trench length, for a fixed jetting configuration.

Some results were published and are given in figure 2.2. The influence of particle size can easily be observed from the figure, where the trench for the medium sand stays open for a longer distance compared to the coarse sand. The trench shapes were extracted from side view images as shown in figure 2.3. Based on the experimental campaign, the following five key processes were identified, see also figure 2.4.

- Erosion
- Deposition (sedimentation)
- Breaching
- Entrainment
- Overspill

Based on the experiments, a model was developed by Vanden Berghe et al. [2011]. However due to a lack of detailed description the proposed model is not directly reproducible.

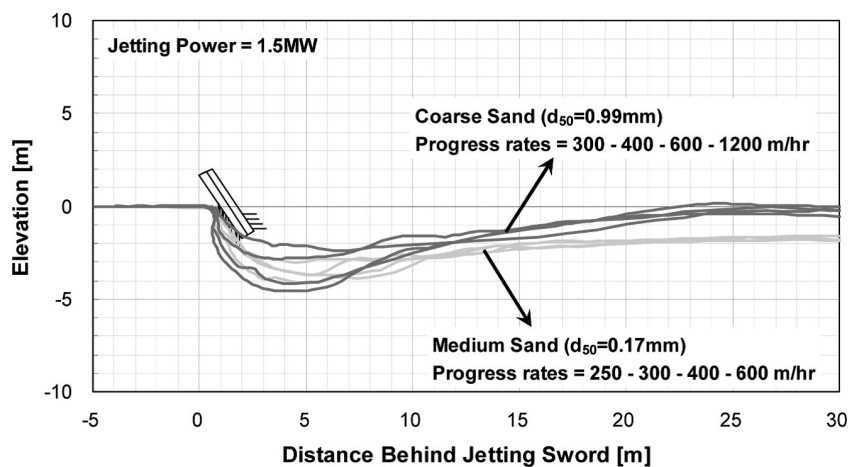


Figure 2.2: Experimental results by [Vanden Berghe et al., 2011], re-scaled from experimental scale to prototype scale.

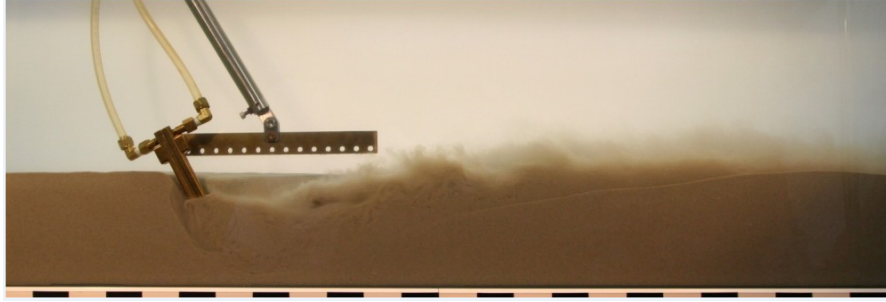


Figure 2.3: Side view of waterjet trenching experiments, carried out at the National University of Taiwan in collaboration with CTC Marine Projects and Fugro Engineers SA [Vanden Berghe et al., 2008].

2.2. Seabed features

Due to the action of tides, currents and waves seabed formations can be formed in sandy seabeds. In literature various terms are used for these seabed formations, e.g. sand waves, sand dunes, ripples and megaripples. Several classifications of these terms exist, based on distinction of dimensions (length and height), for example by Ashley [1990] or Gass [1984]. Throughout this thesis the nomenclature suggested by Gass [1984] is mainly adopted, see table 2.1. However, a general reference to seabed formations is meant by '*sand dunes*'.

Table 2.1: Nomenclature for seabed formations, suggested by Gass [1984].

	Ripples	Megaripples	Sandwaves	Sandbanks
Height [m]	< 0,1	0.4 - 1.5	1.5 - 25	5 - 50
Length [m]	< 0.6	0.6 - 30	30 - 500	Single feature

Normally seabeds consist not only of one grain size, but of a range of particle sizes defined in the particle size distribution (PSD). Small grains behave differently to hydrodynamic forcing than large grains. Due to this fact grain sorting is observed in ripples and sand waves. At the crest of the dunes coarse and well-sorted sediments are observed. In the troughs fine grained and poorly sorted sediment is accumulated. These conclusions are based on both laboratory experiments and field measurements, see Foti and Blondeaux [1995] and Roos et al. [2007].

2.3. Physical processes during jet trenching

From the experiments by Vanden Berghe et al. [2011], five key processes were identified as governing in the trenching process, see figure 2.4. In literature there are clear descriptions of all these processes, except for overspill which is excluded. These remaining four processes are described in detail in section 2.3.2 to 2.3.5. In addition to these four, bed friction is also described in this section to complete the flow description, see section 2.3.6.

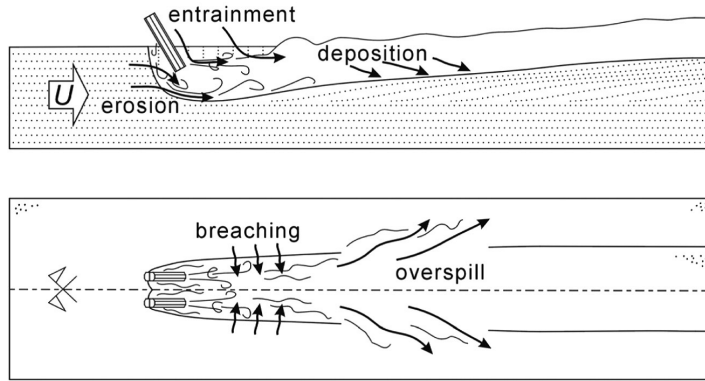


Figure 2.4: Key physical processes during jet trenching [Vanden Berghe et al., 2011].

2.3.1. Dimensionless numbers

There are two dimensionless numbers important for stratified flows where turbulence is not considered [Konblach, 1999]. The first one is the densimetric Richardson number, Ri , which is the ratio of the buoyancy term to the shear term. It can be considered as a measure of stratification in a flow, with large Richardson numbers indicating highly stratified flows. The Richardson number is given by equation 2.1 where g' is the reduced gravity, h the flow height and u the flow velocity.

$$Ri = \frac{g' \cdot h}{u^2} \quad (2.1)$$

Where the reduced gravity is defined with mixture density ρ_m and water density ρ_w in a two-layer system flow by equation 2.2.

$$g' = g \frac{\rho_m - \rho_w}{\rho_w}. \quad (2.2)$$

The second important dimensionless number is the densimetric Froude number (eq. 2.3), which is the ratio of flow velocity to velocity at which a disturbance propagates. When $Fr \leq 1$, the flow is called subcritical and disturbances can travel both up- and downstream. For $Fr \geq 1$ the flow is called supercritical and disturbances can travel only downstream. The transition from supercritical to supercritical flow is often accompanied by a hydraulic jump.

$$Fr = \frac{u}{\sqrt{g' \cdot h}} \quad (2.3)$$

$$Ri = \frac{1}{Fr^2} \quad (2.4)$$

2.3.2. Erosion

When the shear stress generated by a flow velocity is higher than a critical threshold value, particles are removed from the bed. This process is called erosion and can be described by a series of (empirical) expressions. The erosion velocity is defined as the downward directed velocity of the interface between sand bed and flow, and is given by equation 2.5.

$$v_e = \frac{E}{\rho_s(1 - n_0 - c)} \quad (2.5)$$

Where E is the pick-up flux, given by equation 2.6, ρ_s sediment density, n_0 the bed porosity, c the sediment concentration in the flow and $\Delta = (\rho_s - \rho_w) / \rho_w$.

$$E = \Phi_p \cdot \rho_s \sqrt{g \cdot \Delta \cdot d} \quad (2.6)$$

The pick-up flux can be determined via an empirical pick-up function. Although several functions exist, throughout this thesis the pick-up function of van Rijn [1984] is used since this is a well-known and commonly used equation in literature. The pick-up flux in dimensionless form is given by equation 2.7.

$$\Phi_p = 0.00033 \cdot D_*^{0.3} \left(\frac{\theta - \theta_{cr}}{\theta_{cr}} \right)^{1.5} \quad (2.7)$$

Where Φ_p is the dimensionless pick-up flux, D_* the dimensionless particle diameter, θ the dimensionless shear stress (also referred to as the Shields parameter) and θ_{cr} is the critical dimensionless shear stress. The dimensionless particle diameter is given by equation 2.8, where d is particle diameter, Δ specific gravity and ν kinematic viscosity.

$$D_* = d \sqrt[3]{\frac{\Delta \cdot g}{\nu^2}} \quad (2.8)$$

Particles will start to move when the dimensionless shear stress exceeds the critical value (i.e. $\theta > \theta_{cr}$). The Shields parameter is calculated via equation 2.9, where \bar{u} is the depth averaged flow velocity and f_0 the friction coefficient.

$$\theta = \frac{f_0 \cdot \bar{u}^2}{8 \cdot \Delta \cdot g \cdot d} \quad (2.9)$$

To complete the description of the erosion velocity, θ_{cr} is given by equation 2.10. This is one of the numerous functions to describe the critical Shields value, [Brownlie, 1981].

$$\theta_{cr} = 0.22 \cdot R_p^{-0.6} + 0.06 \cdot \exp(-17.77 \cdot R_p^{-0.6}) \quad (2.10)$$

R_p is the particle Reynolds number, but instead of using the settling velocity w_s as in section 2.3.3 for R_p , now the Reynolds particle number is taken by using $\sqrt{\Delta \cdot g \cdot d}$. The particle Reynolds number, used in the critical shear stress equation by [Brownlie, 1981], is given in equation 2.11.

$$R_p = \frac{d \sqrt{\Delta \cdot g \cdot d}}{\nu} \quad (2.11)$$

The above mentioned theory for erosion is derived and calibrated for low flow velocities and low sediment concentrations above the bed. van Rhee [2010] showed that when $v_e / k_l > 3$, the erosion process is considered to be high speed and the existing theory must be adapted. The standard critical shear stress θ_{cr} is multiplied by a term accounting for a sloping surface and the effect of dilatency, see equation 2.12.

$$\theta_{cr}^1 = \theta_{cr} \left(\frac{\sin(\phi - \beta)}{\sin \phi} + \frac{v_e (n_l - n_0)}{k_l (1 - n_l)} \frac{1}{\Delta(1 - n_0)} \right) \quad (2.12)$$

Where β is the surface slope, k_l the permeability of the upper layer and n_l the porosity of the upper layer. The adopted pick-up function is now given by equation 2.13.

$$\Phi_p^1 = 0.00033 \cdot D_*^{0.3} \left(\frac{\theta - \theta_{cr}^1}{\theta_{cr}^1} \right) \quad (2.13)$$

The erosion velocity v_e is now also present in the critical dimensionless shear stress (equation 2.12), therefore it is an implicit relations which can be solved numerically. This expression is given in equation 2.14, which gives the erosion velocity for the high-speed erosion regime, ignoring the sedimentation term.

$$\frac{\Phi_p^1 \sqrt{g \cdot \Delta \cdot d}}{1 - n_0 - c} - v_e = 0 \quad (2.14)$$

2.3.3. Sedimentation

Sand particles settle in clear water due to the density difference of the particles and the water. For increasing velocity of a sand particle also the drag force on the particle is increasing, resulting in an equilibrium velocity of the particle where gravitational and drag force are in balance. The terminal velocity of a single particle, w_0 , is given by equation 2.15 [Ferguson and Church, 2004].

$$w_0 = \frac{\Delta \cdot g \cdot d^2}{C_1 \cdot \nu + \sqrt{0.75 \cdot C_2 \cdot \Delta \cdot g \cdot d^3}} \quad (2.15)$$

Where $C_1 = 18$ and $C_2 = 1$ for natural sand, d is the grain size, Δ is specific gravity and ν is kinematic viscosity. Instead of a single particle, often many particles settle simultaneously. Due to the upward water flow created by the downward going particles, the effective settling velocity is reduced. The effective settling velocity for a large number of particles is dependent on the concentration and can be given by equation 2.16, proposed by [Richardson and Zaki, 1954].

$$w_s = w_0 \cdot (1 - c)^{n_p} \quad (2.16)$$

Where w_0 is the settling velocity of a single particle, c is the concentration and n_p is an exponent dependent on the particles Reynolds number. The exponent is given by equation 2.17, proposed by Rowe [1987] and the particles Reynolds number can be determined with equation 2.18.

$$n_p = \frac{4.7 + 0.41 \cdot R_p^{0.75}}{1 + 0.175 \cdot R_p^{0.75}} \quad (2.17)$$

$$R_p = \frac{w_0 \cdot d}{\nu} \quad (2.18)$$

The sedimentation velocity is defined as the vertical velocity of the interface between settled bed with porosity n_0 and the water sediment mixture above the bed with concentration c . From a volume conservation point of view, equation 2.19 can be derived to give a relation for the sedimentation velocity without considering erosion.

$$v_{sed,s} = \frac{w_s \cdot c}{1 - n_0 - c} \quad (2.19)$$

Together with the erosion flux E from section 2.3.2, the sedimentation velocity for erosion and sedimentation combined is given by equation 2.20. Where S is the sedimentation flux, given by equation 2.21.

$$v_{sed} = \frac{S - E}{\rho_s \cdot (1 - n_0 - c)} \quad (2.20)$$

$$S = \rho_s \cdot w_s \cdot c = \rho_s \cdot w_0 \cdot c \cdot (1 - c)^{n_p} \quad (2.21)$$

2.3.4. Breaching

The maximum slope angle of a cohesionless sand slope is equal to the internal friction angle, when no external forces are considered. When water is flowing in or out of a slope, an additional seepage force is included, increasing or decreasing the maximum slope angle. When considering the case of a vertical slope, the pore volumes at the edge will have to increase for the sand to fall downward. This increase in pore volume is called dilatancy and can only happen when water flows inward.

A detailed derivation of the forces influencing the breaching process is outside of the scope of this thesis. An important parameter describing the breaching process and relevant for trenching is the active wall velocity, which is the propagation speed of a disturbance on the slope. van Rhee [2015] shows that the active wall velocity is given by

$$v_{wall} = -\frac{k_l}{\Delta n} \Delta \frac{\sin(\phi - \beta)}{\sin(\phi)} (1 - n_0), \quad (2.22)$$

where k_l , Δn , Δ , ϕ and β are the permeability at the loose state, change in porosity, specific density, internal friction angle and slope angle respectively. Unfortunately the values of k_l and Δn are difficult to measure. To avoid using these parameters, van Rhee [2015] showed that $(1 - n_0) k_l / \Delta n \approx 10 k_0$, where k_0 is the in-situ permeability. Rewriting equation 2.22 now gives the more practical equation

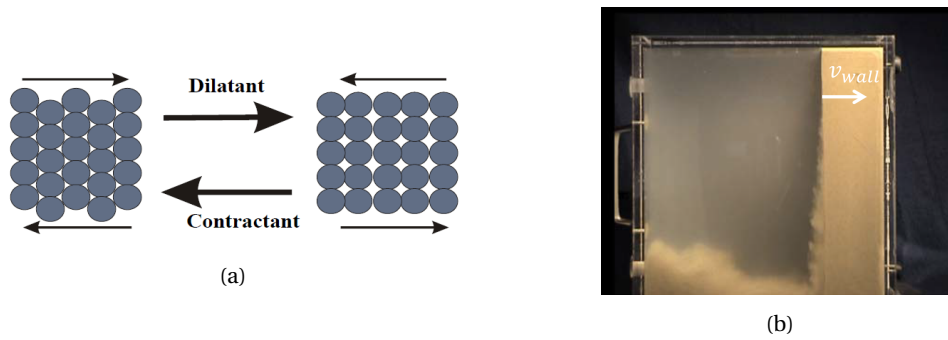


Figure 2.5: (a) Graphical representation of increase in pore volume (dilatancy) and decrease in pore volume (contraction). (b) Demonstration of the breaching process. [van Rhee, 2017]

$$v_{wall} = -10 \cdot k_0 \cdot \Delta \frac{\sin(\phi - \beta)}{\sin \phi}. \quad (2.23)$$

It is not common to test in-situ permeability, k_0 , for offshore wind projects. Therefore it is useful to relate the permeability to another parameter which is known. A practical formula therefore is that of den Adel [1987] which relates the permeability to porosity n and particle size D_{15} , which can be extracted from the particle size distribution. The permeability is given by

$$k_0 = \frac{g}{160 \cdot \nu} D_{15}^2 \frac{n_0^3}{(1 - n_0)^2} \quad (2.24)$$

where ν is the kinematic viscosity.

2.3.5. Entrainment

When a layer of fluid flows through a quiescent body of fluid, there is a transport of fluid through the interface between these two fluids. This transport is commonly known as entrainment, and is governed by entrainment coefficient α_E . For entrainment between two layers with equal density, a value of $\alpha_E = 0.075$ is often assumed [Parker et al., 1987]. However, for stratified flows in which there is a density difference between the two layers this is not valid. For stratified flows the entrainment coefficient is dependent on the stratification, indicated by the Richardson number, see section 2.3.1. Parker et al. [1987] proposed an empirical equation (equation 2.25) which approaches 0.075 for $R_i \rightarrow 0$. Other relations are given in Mastbergen and Berg [2003] (equation 2.26) and Parker et al. [1986] (equation 2.27). The entrainment coefficient is plotted for a range of Richardson numbers in figure 2.6 for each of the previously mentioned empirical relations.

$$\alpha_E = \frac{0.075}{(1 + 718 \cdot Ri^{2.4})^{0.5}} \quad (2.25)$$

$$\alpha_E = \frac{0.0015}{Ri} \quad (2.26)$$

$$\alpha_E = \frac{0.00153}{0.0204 + Ri} \quad (2.27)$$

2.3.6. Bed friction

The shear stress between a flow layer and seabed, is given by τ_b and can be related to the mean flow velocity u via the fluid density and Darcy-Weisbach friction factor f . Bed friction is relevant to determine the external force on a water body, and is an important parameter to determine the erosion velocity of a sediment bed. The bed shear stress is given by equation 2.28.

$$\tau_b = \frac{f}{8} \cdot \rho \cdot u^2 \quad (2.28)$$

For some applications in fluid mechanics, for instance in shallow water flow, it is more practical to define the bed friction by the friction velocity u_* , which is related to the shear stress via equation 2.29.

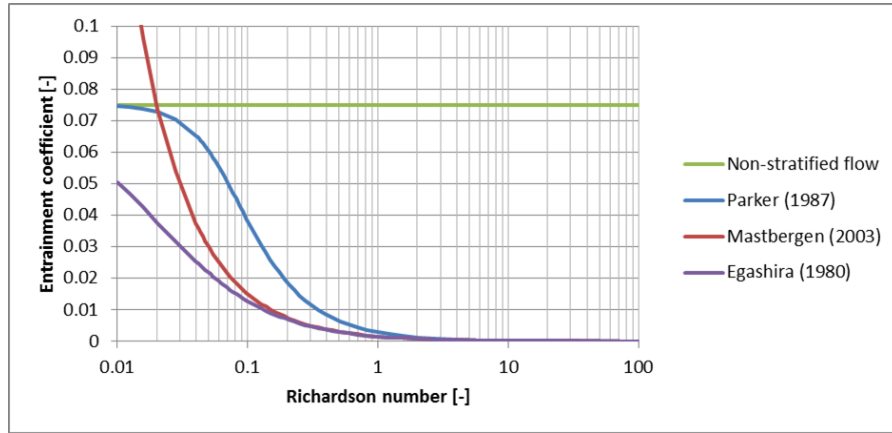


Figure 2.6: Entrainment coefficient as a function of Richardson number for various empirical relations.

$$u_* = \sqrt{\frac{\tau_b}{\rho}} = \sqrt{\frac{f}{8}} \cdot u \quad (2.29)$$

2.4. Free turbulent jets

To understand the working principle of the jet swords, it is important to understand the behaviour of a free circular turbulent jet. Herein we assume that there are no objects obstructing the flow and that the fluid properties of the jet are equal to that of the surrounding water. Furthermore the jet exit velocity u_0 is assumed to be uniform at the nozzle exit. Mixing occurs at the interface between jet and surrounding water, resulting in a transfer of mass and momentum. Ambient water is accelerated in the jet flow, resulting in a deceleration of the jet velocity. As the mixing layer grows with distance from jet exit, eventually the initial velocity core vanishes. The region where this potential core still exists is called the flow development region. The region onward is referred to as the region of fully developed flow, see figure 2.7.

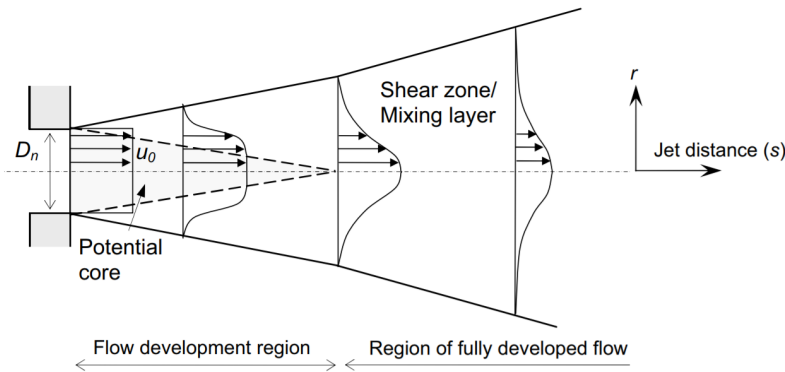


Figure 2.7: Sketch showing the flow field of a circular turbulent jet, including the corresponding definitions. Image from [Nobel, 2013].

By applying the Bernoulli theorem and under the assumption that the jet exit velocity is much larger than the upstream velocity, the exit velocity u_0 can be calculated based on the pressure difference over the nozzle (Δp). The jet exit velocity is given by equation 2.30.

$$u_0 = \sqrt{\frac{2 \cdot \Delta p}{\rho_w}} \quad (2.30)$$

Since normally not the entire cross section of the nozzle diameter used by the jet flow, the diameter D_n is corrected by contraction coefficient α_{con} . The resulting flow rate is given by equation 2.31.

$$Q_j = (\alpha_{con} \cdot D_n)^2 \frac{\pi}{4} \sqrt{\frac{2 \cdot \Delta p}{\rho_w}} \quad (2.31)$$

The fully developed flow region starts at an axial distance of approximately $6.2 \cdot D_n$. In this region, the velocity development along radial distance r and axial distance s is given by equation 2.32.

$$u_j(r, s) = u_0 \sqrt{\frac{k_1 D_n}{2} \frac{r^2}{s}} e^{k_2 \frac{r^2}{s^2}} \quad (2.32)$$

Where k_1 and k_2 are empirical coefficients, equal to $k_1 = 77$ and $k_2 = 87.3$ [Nobel, 2013]. The resulting velocity development along the jet centerline is given in figure 2.8, where the potential core of the jet can be observed, extending to a distance of $6.2 \cdot D_n$.

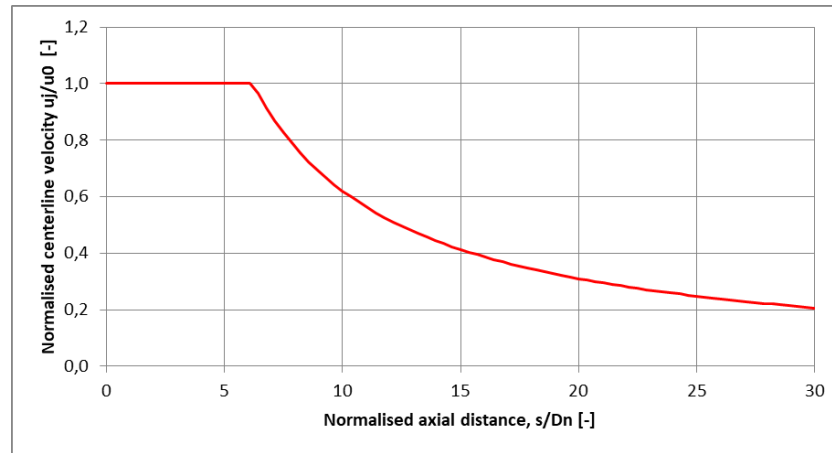


Figure 2.8: Velocity development along jet centerline.

2.5. Jetting in sand

Jetting in sand has extensively been investigated by companies in the dredging industry, however to protect their intellectual property not much has been published. Some theory that is freely available is described in the following sections.

2.5.1. Stationary jetting in sand

Kobus et al. [1979] performed experiments with a stationary jet above a sand bed. Two different regimes were found to develop, resulting in two different scour hole shapes, see figure 2.9. Which of the two scour holes will form can be predicted by using pressure parameter $k_{0,pp}$ (equation 2.33).

$$k_{0,pp} = \frac{p_j}{\frac{1}{2} \rho_w \cdot w_s^2} = \frac{u_0^2}{w_s^2} \quad (2.33)$$

Where p_j is jet pressure, w_s is particle settling velocity and u_0 is jet exit velocity. When $1.2 < k_{0,pp} < 3.0$ a scour hole of form I will develop, and for $k_{0,pp} > 6.5$ scour hole of form II will develop. Form I is characterised by a jet flow that is and stays attached to the crater until it reaches the edge of the crater at $r = r_0$. Form II is characterised by large bed deformation at the center with steep slopes, and an outer area where the slope is straight and dependent on the internal friction angle of the sand [Kobus et al., 1979].

2.5.2. Jetting in sand by a translating jet

Perng and Capart [2008] conducted experiments with a wide jetting beam, simulating the working principle of a water injection dredger. The resulting plane turbulent jet was considered to be fully two-dimensional. Just as for stationary jetting in sand different patterns can be observed from the experiments (figure 2.10), but now for fixed jetting parameters it is dependent on the trail speed of the jetting beam.

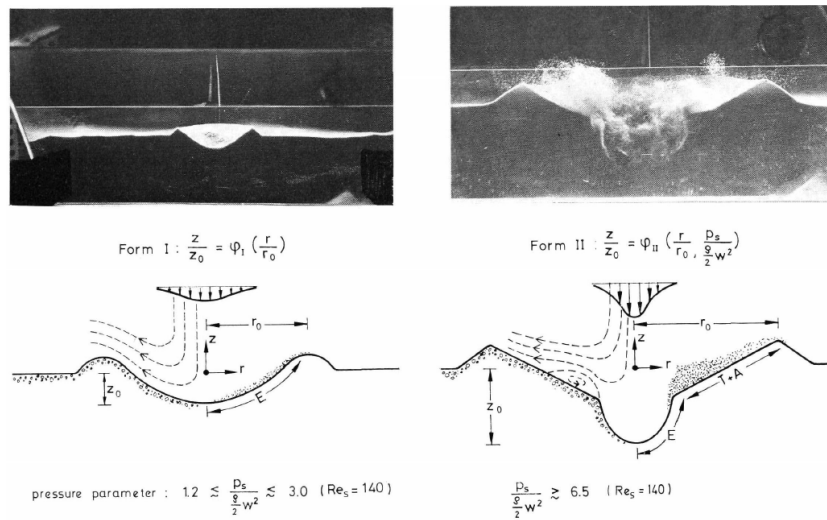


Figure 2.9: Two different options of scour hole profiles for stationary jets, depending on pressure parameter p_p [Kobus et al., 1979].

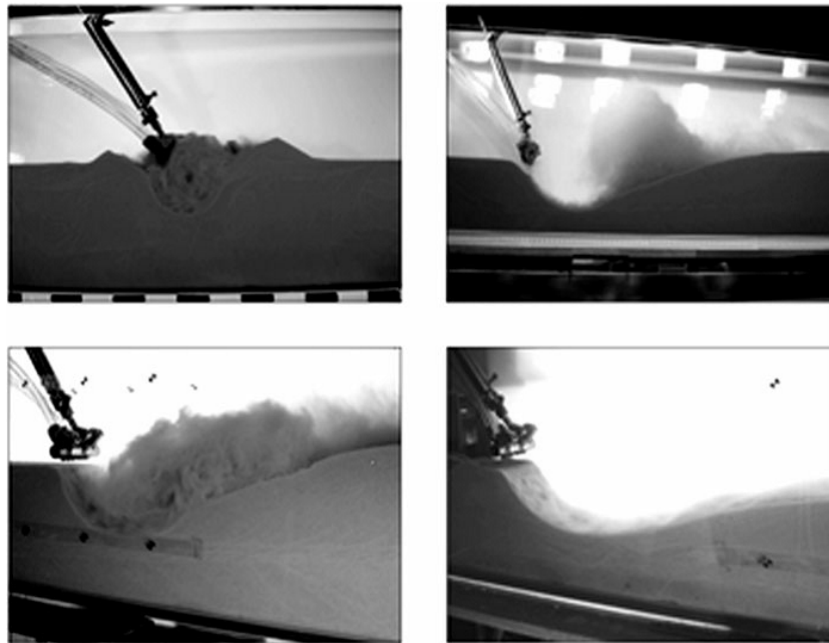


Figure 2.10: Qualitative comparison of trench profiles create by a plane turbulent jet, for varying trailing speeds. Top left; stationary jet, top right; very slowly moving jet, bottom left; slowly moving jet, bottom right; rapidly moving jet. Image by Perng and Capart [2008].

For the very slowly travelling jet (figure 2.10 top right), breaching is reported to occur in the upwind direction of movement near the impingement point of the jet. For faster trailing speeds this breaching does not occur, possibly due to the effect of water inflow due to dilatency [Perng and Capart, 2008]. During the experiments with a slowly travelling jet a hydraulic jump was observed, see bottom left in figure 2.10. For the rapidly moving jet a more shallow, elongated profile is observed. The sediment remains confined in the shallow layer flowing over the bed.

2.5.3. Jet production - Specific energy approach

Miedema [2015] proposed a model for the in-situ production of jets in a draghead. It is based on the assumption that the specific energy required to fluidise sand is equal to the specific energy required to cut sand with a blade, having a small blade angle and at zero meter waterdepth. For deep water this assumption does not hold since soil cutting is influenced by cavitation, thus dependent on absolute water pressure. Whereas the jet production is dependent on pressure difference, thus relative pressure.

Let's assume a trench with depth H and width W , the in-situ production Q_s can be determined by including trenching speed v_t . The in-situ production is defined as the total volumetric flow rate (sand and pore water).

$$Q_s = A \cdot v_t \quad (2.34)$$

The in-situ production (sand plus pore water) of the trencher can also be given by dividing the installed jet power P_j by the specific energy E_{sp} . Which results from rewriting the definition of specific energy, see section 2.7.

$$Q_s = \frac{P_j}{E_{sp}} \quad (2.35)$$

The total jet power is found by multiplying the pressure difference Δp_j with the amount of nozzles n_j , the jet exit velocity and nozzle cross section. Jet exit velocity is found via the Bernoulli theorem. Furthermore the diameter is compensated by contraction coefficient α_c , to obtain the correct flow rate.

$$P_j = p_j \cdot n_j \sqrt{\frac{2 \cdot p_j}{\rho_w} \frac{\pi}{4}} (\alpha_c \cdot D_j)^2 \quad (2.36)$$

The specific energy is now determined by assuming it is equal to that of non-cavitating cutting. This results in the following equation where ε is dilatancy, k_m mean permeability. The horizontal force coefficient c_1 must be calibrated using experiments. Miedema [2014] suggests a value of 0.12, found by calibrating to a series of experiments done by "Combinatie Speurwerk Baggertechniek", published in [de Jong, 1988].

$$E_{sp} = c_1 \cdot \rho_w \cdot g \cdot h_i \cdot v_t \frac{\varepsilon}{k_m} \quad (2.37)$$

For cutting soil with a blade the parameter h_i is the layer thickness. This can be related to jet trenching, by setting h_i equal to trench depth. The ratio of mean permeability to dilatancy can be approximated using the Kozeny Carman equation, resulting in the following equation, where k_i is the initial permeability.

$$\frac{k_m}{\varepsilon} \approx 10 \cdot k_i \quad (2.38)$$

Combining all previous equations gives the following equation for the maximum trench cross section A .

$$A = \frac{p_j \cdot n_j \sqrt{\frac{2 \cdot p_j}{\rho_w} \frac{\pi}{4}} (\alpha_c \cdot D_j)^2 10 \cdot k_i}{c_1 \cdot v_t^2 \cdot \rho_w \cdot g \cdot h_i} \quad (2.39)$$

2.5.4. Jet production - C.S.B.

Research by "Combinatie Speurwerk Baggertechniek" (CSB) on the production of sand by jets resulted in a data set and corresponding empirical equations [de Jong, 1988]. The research was aimed at the production of jets in dragheads, having a transverse velocity in the range of 0.5-2 m/s. Typical trencher speeds are between 0.05-0.2 m/s, thus being considerably lower. The penetration depth of a single jet is given by d , and width is indicated as a fraction of d ($\alpha_{CSB} \cdot d$). The empirical equation for in-situ sand production by a single jet is given below.

$$Q_s = \frac{\alpha_{CSB} \cdot 3.295 \cdot 10^{-7} \cdot p_j^{1.18} \cdot D_j^{0.98} \cdot d_{50}^{1.722}}{v_t} \quad (2.40)$$

To be able to compare to the other jet production models, the equation is re-written in terms of a trench area A and multiplied by the total number of nozzles n_j .

$$A = \frac{\alpha_{CSB} \cdot n_j \cdot 3.295 \cdot 10^{-7} \cdot p_j^{1.18} \cdot D_j^{0.98} \cdot d_{50}^{1.722}}{v_t^2} \quad (2.41)$$

When applying this equation on the jet swords it is assumed that the nozzles are perfectly divided over the trench cross section, which is probably not the case. Furthermore coefficient α_{CSB} is unknown. CSB found α_{CSB} values between 0.5 and 2.2, with low α_{CSB} values corresponding to low transit velocities and high α_{CSB}

values to high transit velocities, see figure 2.11. For the trenching speeds considered (0.07 m/s), an α_{CSB} value of 0.07 is expected when extrapolating this trend.

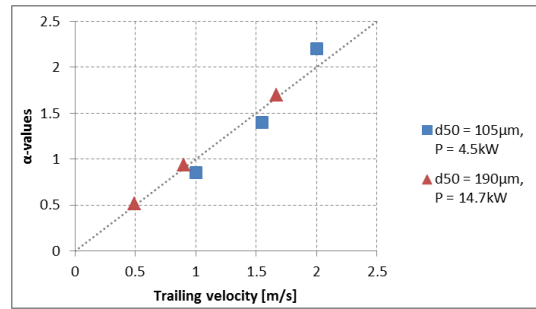


Figure 2.11: Trench shape ratio α_{CSB} as a function of the transit velocity v_t for two different soil type and hydraulic power combinations. Data points are from research by CSB de Jong [1988].

2.5.5. Jet production - Vlasblom

A simple expression for the production of water jets was given by Vlasblom [2003]. It is based on experimental data which has not been made public, and developed for jets present on trailing dragheads. The equation (2.42) states that the jet production, defined as the eroded sand mass per unit time, is linearly dependent on the jet momentum I .

$$\dot{M}_s = \alpha_{vl} \cdot I_j = \alpha_{vl} \cdot \rho_w \cdot Q_j \cdot u_0 = \alpha_{vl} \cdot \rho_w \cdot Q_j \sqrt{\frac{2 \cdot p_j}{\rho_w}} \quad (2.42)$$

The mass flux \dot{M}_s can be given in terms of trench cross section, trenching velocity and in-situ soil parameters by equation 2.43.

$$\dot{M}_s = A \cdot v_t \cdot (1 - n_0) \cdot \rho_s \quad (2.43)$$

Rewriting this equation to give the maximum trench cross section results in equation 2.44.

$$A = \frac{\alpha_{vl} \cdot \rho_w \cdot Q_j \sqrt{\frac{2 \cdot p_j}{\rho_w}}}{v_t \cdot (1 - n_0) \cdot \rho_s} \quad (2.44)$$

The coefficient α_{vl} , which has unit time over length, requires some explanation. Vlasblom stated it is a "coefficient depending on the particle size, jet pressure, jet capacity and trail speed", with a reasonable assumption of $\alpha_{vl} = 0.1$. Experiments have been done by Weegenaar Weegenaar et al. [2015] to validate the formula by Vlasblom. Values for the α_{vl} coefficient were found to be around 0.13-0.14 s/m.

2.5.6. Comparison jet production models

The three jet production models mentioned before in section 2.5.3, 2.5.4 and 2.5.5 are all written as a maximum trench cross section. When considering a required trench depth of 1.8m and width of 0.6m, the maximum trencher velocity can be calculated for each model, see figure 2.12. Soil and jetting parameters considered are a jet pressure of $p_j = 8\text{bar}$, contraction coefficient $\alpha_c = 0.85$, nozzle diameter $D_j = 14\text{mm}$, number of nozzles $n_j = 28$, initial permeability of $k_i = 0.0001\text{m/s}$, porosity $n_0 = 0.35$ and median grain size $d_{50} = 130\mu\text{m}$.

From figure 2.12 it can be concluded that all three models show similar trends. However there is quite some spread in the maximum trencher velocity allowed to produce a 2.0m by 0.75m trench, namely between 500 and 700m/hr.

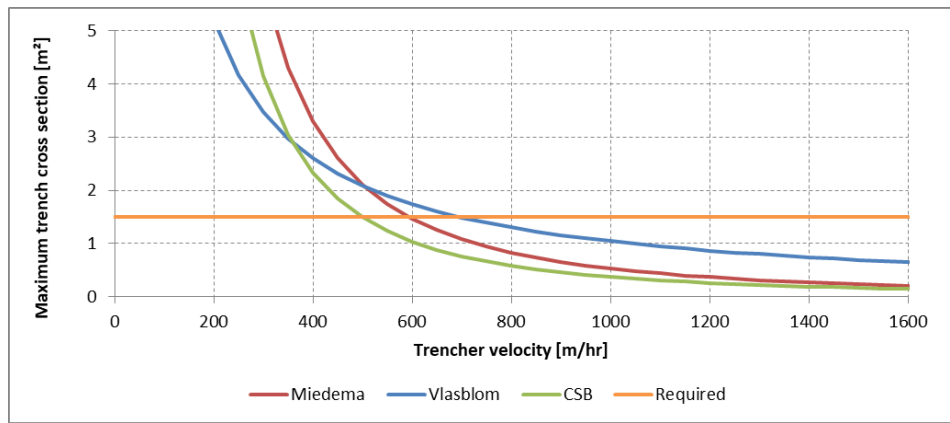


Figure 2.12: Maximum trench cross section for the Miedema, CSB and Vlasblom jet production models. Required trench cross section based on a 2m by 0.75m trench.

2.6. Soil mechanics

2.6.1. Mohr-coulomb failure criteria

The maximum shear strength of a soil can be calculated with the Mohr-Coulomb failure criterion. See equation 2.45, where τ is the maximum shear strength, c is the cohesion or internal shear strength and ϕ is the angle of internal friction. Sand can be considered as a purely frictional soil where $c = 0$ is often assumed.

$$\tau = c + \sigma \cdot \tan(\phi) \quad (2.45)$$

The failure criterion of a soil with both cohesion and friction can be graphically represented as in figure 2.13.

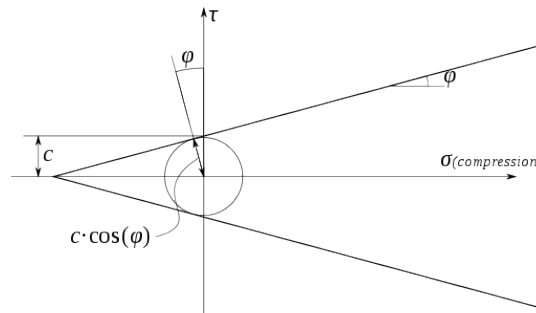


Figure 2.13: Mohr-Coulomb failure envelope for a soil with both cohesion and friction.

2.6.2. Shear stress-displacement behaviour

To characterise the thrust-slip behaviour of tracked vehicles on soil, it is important to understand the shear stress-displacement relationship. Generally there are three distinct types of shear stress-displacement behaviour, each type is elaborated below.

Type 1

For the first type, the shear stress increases with shear displacement, until it approaches a maximum (τ_{max}). Loose sand is an example of a soil showing this type of behaviour [Bekker, 1956]. This relation can be described with equation 2.46, where j is the shear deformation, τ_{max} is the maximum shear stress (see section 2.6.1) and K_1 is often referred to as the shear deformation modulus and indicates the amount of shear deformation required to develop the maximum shear stress.

$$\frac{\tau}{\tau_{max}} = 1 - \exp(-j/K_1) \quad (2.46)$$

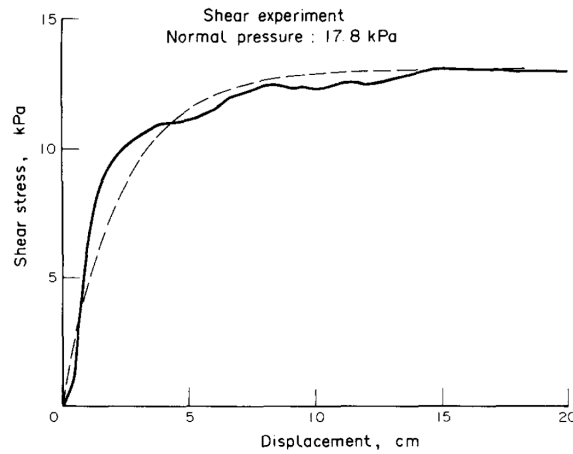


Figure 2.14: Shear stress-displacement curve for a loose sand (type 1) [Wong and Preston-Thomas, 1983].

Type 2

The second type is different from loose soil, it rather quickly reaches a peak after which the original structure of the soil is destroyed and there is a rapid decrease in shear stress [Bekker, 1956]. This relation is described by equation 2.47 where K_2 again indicates the required displacement to achieve the maximum shear strength ($j = K_2$ when $\tau = \tau_{max}$).

$$\frac{\tau}{\tau_{max}} = (j/K_2) \cdot \exp(1 - j/K_2) \quad (2.47)$$

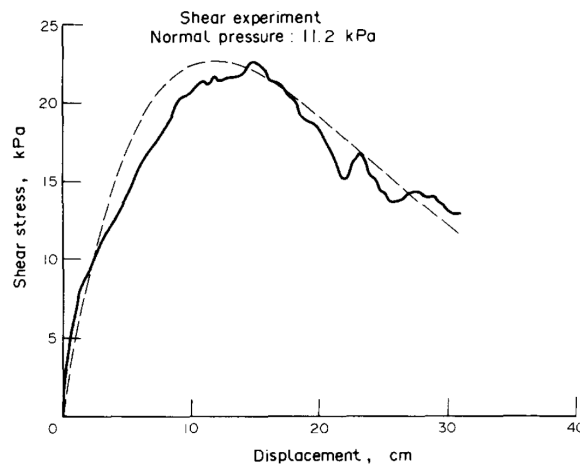


Figure 2.15: Shear stress-displacement curve (type 2) [Wong and Preston-Thomas, 1983].

Type 3

The third type of shear stress-displacement behaviour can be considered a combination of the first two types. Initially it peaks at the maximum shear stress, after which it decreases to approach the residual shear stress, see figure 2.16. Various relations are suggested in literature, however only the one of Wong and Preston-Thomas [1983] is presented here in equation 2.48. Where K_r and K_w are empirical parameters to be fitted on a measured curve.

$$\frac{\tau}{\tau_{max}} = K_r \cdot \left(1 + \left(\frac{1}{K_r \cdot (1 - \frac{1}{e})} - 1 \right) \cdot \exp(1 - j/K_w) \right) \cdot (1 - \exp(-j/k_w)) \quad (2.48)$$

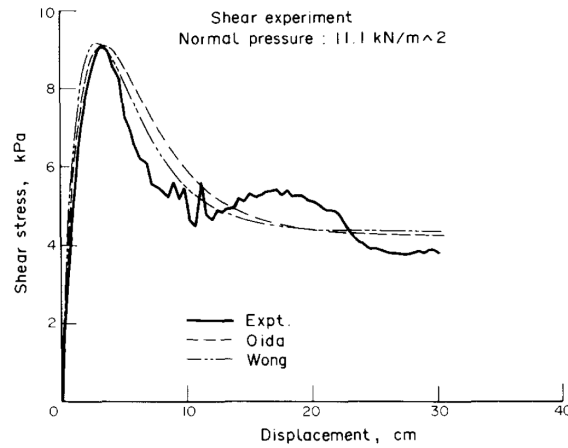


Figure 2.16: Shear stress-displacement curve (type 3) [Wong and Preston-Thomas, 1983].

As throughout this thesis sand dunes are considered, normally containing loosely packed sand, the relationship of type 1 is assumed.

2.6.3. Soil stress distribution under uniform strip load

Boussinesq [1885] derived a theory for the distribution of surface stresses in a soil mass. The soil is assumed to be a homogeneous, isotropic, linear elastic material. Analytical solutions for various type of surface stresses exist (e.g. point load, line load, strip load). Each track belt of the trenching vehicle can be considered as a strip load with width B . The horizontal ($\Delta\sigma_x$) and vertical stress ($\Delta\sigma_z$), indicated in figure 2.17, are given by equation 2.49 and 2.50.

$$\Delta\sigma_x = \frac{q_s}{\pi} (\alpha - \sin(\alpha) \cdot \cos(\alpha + 2\beta)) \quad (2.49)$$

$$\Delta\sigma_z = \frac{q_s}{\pi} (\alpha + \sin(\alpha) \cdot \cos(\alpha + 2\beta)) \quad (2.50)$$

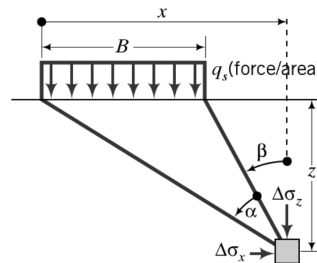


Figure 2.17: Stress distribution under uniform strip load.

2.7. Specific energy

Specific energy, denoted by E_{sp} , is a useful parameter to estimate the production of sand, clay or rock based on available cutting power, often used in the dredging industry. The definition used in the dredging industry is:

“The amount of energy, that has to be added to a volume unit of soil (e.g. sand, clay or rock) to excavate the soil.” [Miedema, 2014]

Based on the definition above, the mathematical description of specific energy is given by equation 2.51, where P_c is the cutting power and Q_c is the volumetric production.

$$E_{sp} = \frac{P_c}{Q_c} \quad (2.51)$$

2.8. Track belt theory

2.8.1. Rigid versus flexible track belts

Track belt driven vehicles can be categorised in two main types; flexible and rigid. With their distinction made by suspension stiffness, see figure 2.18. Flexible tracks have rollers mounted on a suspension, which can be either a vertical translating springs or a pivot arm type of suspension. Tracks consist of links with a short length or rubber belts. Generally the speed of this type of tracked vehicle is high, for example military type or off-road transport vehicles.

Rigid track belts have rollers mounted in a fixed position, without being able to move vertically. Generally the length of the links connecting the chain are long. As a result the track does not show much vertical displacement, with the intention to create a more uniform ground pressure distribution. This type of track belt is mostly used for slow speed vehicles used in farming and construction (cranes).



Figure 2.18: Flexible type track belt (left) and rigid type track belt (right), image from [Daanen, 2017].

2.8.2. Grousers

Generally all track belts have some sort of profile on the running surface, called grousers. The function of grousers is to provide more traction. This is achieved by ensuring soil failure, rather than soil-track friction. Since normally the internal friction angle is larger than the external friction angle, the maximum amount of traction is increased. Furthermore additional thrust is generated at the vertical friction planes at the sides of the grousers.

2.8.3. Slip

When a tracked vehicle is driving over ground, the velocity of the track belt is often different from the speed of the vehicle over ground. This mechanism is referred to as slip and is expressed by the slip ratio. The slip ratio definition is given by equation 2.52, which shows that the slip ratio is positive when the track speed is larger than the speed over ground.

$$i = 1 - \frac{v_t}{v_{track}} = \frac{v_{track} - v_t}{v_{track}} \tag{2.52}$$

Where i is the slip ratio, v_t the speed of the trencher over ground and v_{track} the track velocity. Due to this difference in track and vehicle velocity a certain amount of shear displacement (j) occurs at the track-ground interface. This shear displacement varies linearly from $j = 0m$ at the front of the track to $j = i \cdot L$ at the end of the track with length L . The shear displacement along track length is given by equation 2.53, where x is the coordinate along track belt length, see figure 2.19.

$$j(x) = i \cdot x \tag{2.53}$$

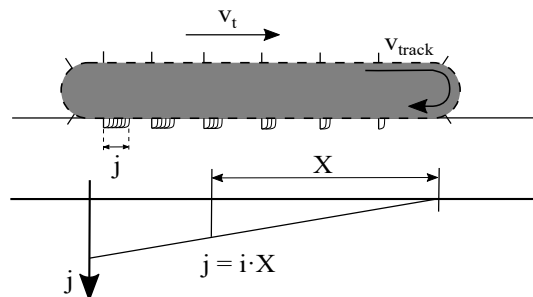


Figure 2.19: Visualisation of shear displacement initiated by a difference in track and trencher velocity.

2.8.4. Slip sinkage

Slip sinkage, defined as the increase in vehicle sinkage due to slip, was recognised over 50 years ago by Reece [1965]. The slip sinkage mechanism is different from static sinkage. Slip sinkage can be seen as “*the mechanical removal of soil by scoops or blades*” [Bekker, 1956], resulting in the digging-in phenomena due to the removal of soil underneath the tracks. Three different relations are given below in equation 2.54 by Bekker [1956], equation 2.55 by Reece [1965] and equation 2.56 by Lysako [2009]. A comparison of these relations is given in figure 2.20, where the total sinkage for each relation is plotted.

$$Z_i = 2 \cdot h_{gr} \cdot i \quad (2.54)$$

$$Z_i = \frac{h_{gr} \cdot i}{1 - i} \quad (2.55)$$

$$Z_i = \left(\frac{1 + i}{1 - 0.5 \cdot i} - 1 \right) \cdot Z_0 \quad (2.56)$$

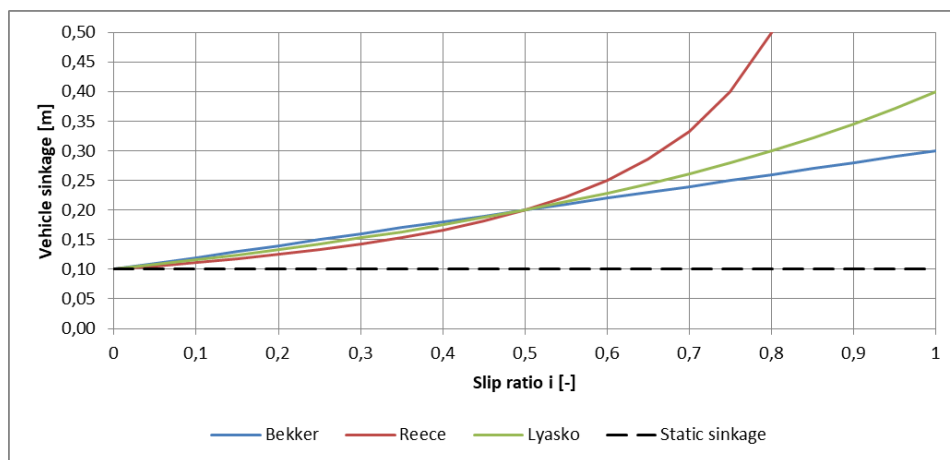


Figure 2.20: Comparison of the slip sinkage relations proposed by Bekker [1956], Reece [1965] and Lysako [2009] for a static sinkage depth of $Z_0 = 0.1\text{m}$ and grouser height of $h_{gr} = 0.1\text{m}$.

3

Jet trenching model

Not available

4

Traction model

Not available

5

Results and discussion

Not available

6

Conclusions and recommendations

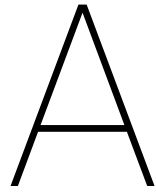
Not available

Bibliography

- Ashley,G. Classification of large-scale subaqueous bedforms: a new look at an old problem. *Journal of Sedimentary Petrology*, 60:160–172, January 1990.
- Bekker,M.G. *Theory of land locomotion: The mechanics of vehicle mobility*. University of Michigan press, 1956.
- Boussinesq,J. Application des potentiels a l'étude de le l'équilibre et du mouvement des solides élastiques. 1885. Gauthier-Villars.
- Brownlie,W.R. Prediction of flow depth and sediment discharge in open channels. Techreport 43A, W. M. Keck Laboratory of Hydraulics and Water Resources, 1981.
- Daanen,E. Mobility of subsea tracked equipment. mathesis, Delft University of Technology, June 2017.
- de Jong,P. Een productie optimalisatie van het gebruik van spuiters op de sleepopperzuiger volvox delta. Master's thesis, Technische Universiteit Delft, 1988.
- den Adel,H. Heranalyse doorlatendheidsmetingen door middel van de forch- heimer relatie (in dutch). Tech Report CO-272550/56, Grondmechanica Delft, Afdeling Waterbouwkundige Constructies, Delft, 1987.
- DNV-GL,. Subsea power cables in shallow water. Recommended Practice DNVGL-RP-0360, Det Norske Veritas AS, March 2016.
- Ferguson,R.I. and Church,M. A simple universal equation for grain settling velocity. *Journal of Sedimentary Research*, 74(6):933–937, nov 2004. doi: 10.1306/051204740933.
- Foti,E. and Blondeaux,P. Sea ripple formation: the heterogeneous sediment case. *Coastal Engineering*, 25(3): 237 – 253, 1995. ISSN 0378-3839. doi: [https://doi.org/10.1016/0378-3839\(95\)00005-V](https://doi.org/10.1016/0378-3839(95)00005-V).
- Gass,I.G. Oceanography: Sediments. *The Open University*, 1984.
- Kobus,H., Leister,P., and Westrich,B. Flow field and scouring effects of steady and pulsating jets impinging on a movable bed. *Journal of Hydraulic Research*, 17(3):175–192, 1979. doi: 10.1080/00221687909499582.
- Konblauch,H. Overview of density flows and turbidity currents. Technical Report PAP-816, Water resources research laboratory, June 1999.
- Lysako,M. Slip sinkage effect in soil-vehicle mechanics. *Journal of Terramechanics*, 47:21–31, 2009. doi: 10.1016/j.jterra.2009.08.005.
- Mastbergen,D.R. and Berg,J.H. Van Den. Breaching in fine sands and the generation of sustained turbidity currents in submarine canyons. *Sedimentology*, 50(4):625–637, jul 2003. doi: 10.1046/j.1365-3091.2003.00554.x.
- Miedema,S.A. *The Delft Sand, Clay and Rock Cutting Model*. IOS Press BV, 1 edition, 2014. ISBN 987-1-61499-453-4.
- Miedema,S.A. *OE4607 Introduction Dredging Engineering*. Delft University of Technology, 2 edition, 2015.
- Nobel,A.J. *On the excavation process of a moving vertical jet in cohesive soil*. PhD thesis, Delft University of Technology, The Netherlands, 2013.
- Parker,G., Fukushima,Y., and Pantin,H. Self-accelerating turbidity currents. *Journal of Fluid Mech.*, 171:145–181, 1986.
- Parker,G., Garcia,M., Fukushima,Y., and Yu,W. Experiments on turbidity currents over an erodible bed. *Journal of Hydraulic Research*, 25(1):123–147, jan 1987. doi: 10.1080/00221688709499292.

- Perng,A.T.H. and Capart,H. Underwater sand bed erosion and internal jump formation by travelling plane jets. *J. Fluid Mech.*, 595:1–43, 2008. doi: 10.1017/S0022112007008567.
- Reece,A.R. Principles of soil-vehicle mechanics. *Proc. Inst. Mech. Eng. Automob. Div.*, 180(1):45–66, 1965.
- Richardson,J. and Zaki,W. Sedimentation and fluidization: Part i. *Trans. Inst. Chem. Engrs*, 32:35–53, 01 1954.
- Roos,P.C., Hulscher,S.J.M.H., and van der meer,F. Grain size sorting over offshore sandwaves: observations and modelling. In *River, Coastal and Estuarine Morphodynamics, RCEM 2007*., pages 649–656, United Kingdom, 9 2007. Taylor & Francis. ISBN 0-415-4536-3-1.
- Rowe,P.N. A convenient empirical equation for estimation of the richardson-zaki exponent. *Chemical Engineering Science*, 42(11):2795 – 2796, 1987. ISSN 0009-2509. doi: [https://doi.org/10.1016/0009-2509\(87\)87035-5](https://doi.org/10.1016/0009-2509(87)87035-5).
- van Rhee,C. Sediment entrainment at high flow velocity. *Journal of Hydraulic Engineering*, 136(9):572–582, 2010. doi: 10.1061/(ASCE)HY.1943-7900.0000214.
- van Rhee,C. Slope failure by unstable breaching. *Proceedings of the ICE - Maritime Engineering*, 168:84–92, 06 2015.
- van Rhee,C. Dredging processes II: lecture notes, February 2017. OE4727.
- van Rijn,L.C. Sediment pick-up functions. *Journal of Hydraulic Engineering*, 110(10):1494–1502, 1984. doi: 10.1061/(ASCE)0733-9429(1984)110:10(1494).
- Vanden Berghe,J.F., Capart,H., and Su,J.C.C. Jet induced trenching operations: Mechanisms involved. *Offshore Technology Conference*, 2008. OTC 19441.
- Vanden Berghe,J.F., Pyrah,J., Gooding,S., and Capart,H. Development of a jet trenching model in sand. *Frontiers in Offshore Geotechnics II*, pages 889–894, 2011.
- Vlasblom,W.J. Designing dredging equipment. Lecture notes (WB3408b), 2003.
- Weegenaar,R.A., Keetels,G.H., Winkelman,M.O., and van Rhee,C. Sand erosion with a traversing circular jet. *Maritime Engineering*, 168:76–83, 2015. doi: DOI:10.1680/maen.14.00004.
- Wong,J.Y. and Preston-Thomas,J. On the characterization of the shear stress-displacement relationship of terrain. *Journal of Terramechanics*, 19(4):225–234, 1983.

Appendices



Trencher specifications (CBT-1100)

Not available

B

Trenching process identification

Not available

C

Results of cable deflection model verification with OrcaFlex

Not available

D

Second pass trenching

Not available